The Research on Accident Tolerant Fuel in CGN

Tong Liu*, Jiaxiang Xue*, Rui Li, Lei Li, Daxi Guo, Qiang Zhang, Duoting Xu

Department of ATF R&D, China Nuclear Power Technology Research Institute Co., Ltd., China General Nuclear Power Corporation (CGN), Shenzhen, 518026, PR China

*Corresponding author.

E-mail addresses: liutong@cgnpc.com.cn; xuejiaxiang@cgnpc.com.cn

Abstract

Under the framework of the national ATF R&D program led by CGN, several types of claddings and pellets with enhanced accident tolerance have been developed for light water reactors, including coated zirconium alloy, iron-chromium-aluminum alloys, coated molybdenum alloy, silicon carbide claddings, as well as high thermal conductivity UO_2 pellets. The out-of-pile performance of these cladding candidates and pellets such as thermal and mechanical properties and high temperature corrosion has been tested. In parallel the economic evaluation and safety analysis have been carried out for typical ATF designs. This paper provides an update on the R&D status and a summary of the results.

1. Introduction

The nuclear disaster at Fukushima Japan in 2011 has strongly aroused public concerns about nuclear safety. In this context, the accident tolerant fuels (ATF) concept was initiated to further extend safety margins and strengthen nuclear safety of light water reactors (LWRs) under accidents beyond design basis (BDB), and even more importantly to rebuild the public confidence to nuclear energy [1-3]. To date, the major nuclear countries such as the United States, France, UK, China, South Korea, etc. have initiated definitive research programs aimed to develop the ATF technology. This technology involves development of a wide range of promising new cladding materials and pellet materials, such as coated Zry[4,5], FeCrAl [6], Mo[7-9], SiC_f/SiC[10] and UO_2-BeO featuring much better accident tolerance and other unique advantages compared to the conventional Zircaloy cladding and UO_2 pellet being served in

current commercial LWRs.

China General Nuclear Power Corporation (CGN) is leading the China accident tolerant fuels (ATF) research program. Under the framework of this program, CGN has also been developing ATF materials. In this paper, the latest progress was reported.

2. Experimental

1. Materials Manufacture

a) Surface-coated Zircaloy

Various coating fabrication techniques and coating candidate materials have been studied to obtain the best processing routes and coating material options. The coating fabrication techniques included physical vapor deposition (PVD), plasma spraying, cold spraying and laser clad. In this paper, we described in detail the Cr coating fabricated by PVD and its properties.

b) FeCrAl and ODS-FeCrAl

FeCrAl alloy and its oxide dispersion strengthened (ODS) versions have been developing, including alloy design and fabrication of thin-walled tubes. The FeCrAl alloy was fabricated by a vacuum arc-melting method, while its ODS versions were consolidated by hot isostatic pressing following mechanical alloying. These two alloys have been successfully manufactured into thin-walled tubes with dimensions of 4m long, 0.3-0.5mm thick and 9.5mm in outer diameter (Figure 1).

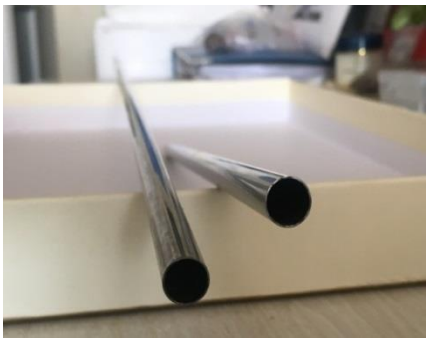

Figure 1: Photo of ODS-FeCrA thin-walled tubes

c) Surface-coated ODS Mo alloy

ODS Mo alloy is composed of Mo and fine particles uniformly dispersed in the Mo matrix. The mechanical properties of the ODS Mo alloy are mainly determined by the

type of the particles, their dispersion homogeneity, contents and sizes. In this study, a special doping process was employed to achieve homogeneous dispersion of the doped oxides in the Mo matrix. So far, ODS Mo thin-walled tubes have been successfully manufactured, with dimensions of 4m long, 0.3-0.5mm thick and 9.5mm in outer diameter (Figure 2). In order to overcome the notorious weak oxidation resistance of Mo, coating was prepared on the Mo surface to prevent severe oxidation.

Figure 2: Photo of ODS-Mo thin-walled tubes

d) SiC_f/SiC composite

SiC_f/SiC composite tubes are consisted of multiple layers, each of which has a different function. The dense matrix layer is designed to ensure good permeability and leak-tightness. Its surface is made to resist high temperature steam oxidation and thus reduce hydrogen generation and oxidation rate. The matrix is reinforced by SiC fibers which are expected to well bear loads. So far, thin-walled **SiC_f/SiC** composite tubes with a length of 1 m have been fabricated in our laboratory (Figure 3).

Figure 3: Photo of thin-walled SiC_f/SiC composite tubes

e) High thermal conductivity UO_2 pellets

Some additives, BeO, SiC, diamond and metal, exhibit high thermal conductivity,

low capture cross section, good neutron moderation, high resistance to water steam and excellent compatibility with UO_2 below 2160 °C. Therefore, these become promising additives to be researched. In this paper, several types UO_2 pellets were produced by normal method and Spark Plasma Sintering (SPS) method, which SPS realizing shorter time and lower sintering temperature and higher thermal conductivity.

Figure 4: Photo of high thermal conductivity UO_2 pellets

2. Test and characterization

The microstructure of the tubes was examined under scanning electron microscope (SEM) and transmission electron microscope (TEM). Mechanical properties such as tensile and three-point-bending strength were tested with a loading rate of 0.5mm/min at room temperature and 1200℃. Water corrosion tests were conducted in autoclave for 72h to study compatibility with static PWR water. High temperature steam oxidation tests were perfomred at 1200℃. The UO_2 pellets density were measured by Archimedes method. The thermal conductivity of pellets was tested by a laser flash apparatus (LFA 427, Netzsch, Germany), and the testing temperature range was 25-1600°C, with an interval of 200°C. Thermal conductivity (λ) was calculated as a function of temperature from the measured thermal diffusivity (α), heat capacity (Cp), and the true density (ρ) according to the equation: $\lambda=\rho\alpha Cp$.

3. Results and discussion

a) Surface-coated Zircaloy

The oxidation tests under 1200℃ steam were performed using DSC-TG technique to evaluate oxidation resistance of different coating candidates. The results show that Cr

coating prepared by PVD is the best option in contrast to FeCrAl which did not protect the matrix. SEM observations at the cross-sections of the FeCrAl coated sample show that the coating was subjected to laminar oxidation, i.e. Zr is present at the surface of the coating, resulting from absence of Cr_2O_3 and Al_2O_3 oxide films (Figure 5). This phenomenon is attributed presumably to eutectic reactions of Zr and Fe at 900℃, leading to rupture of the coating. By contrast, the results of the oxidation tests of the Cr, CrN and CrAl coated Zircaloy show much better resistance to high temperature steam environment.

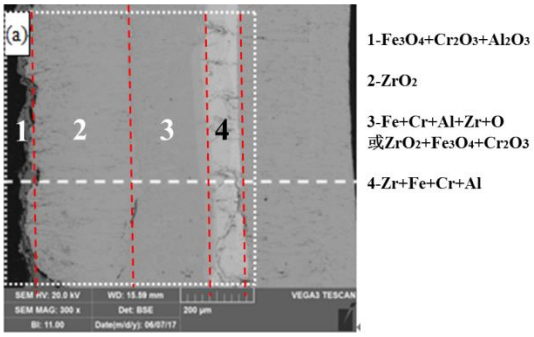

Figure 5: SEM images of cross-section of a FeCrAl-coated Zry sample

In addition, the autoclave test results in Figure 6 show that the weight gain of coated Zircaloy is only less one half of that observed at bare Zircaloy, indicating good water corrosion resistance of the coatings. From the surface appearances of samples after autoclave water corrosion tests, it can be found that the bare Zircaloy sample was turned into black, which is a typical color after water corrosion. By contrast, the Cr and CrN coated Zircaloy samples remained the metallic luster indicating no obvious corrosion. The CrAl coated Zircaloy samples shown dark gray, indicating that the surface was not smooth and dense.

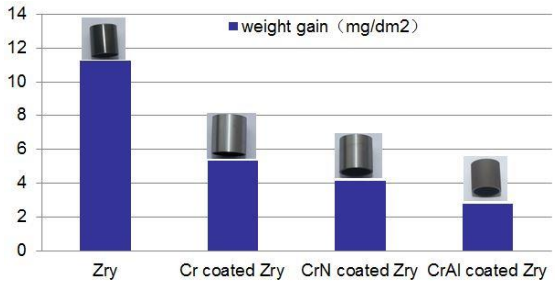

Figure 6: Comparison of oxidation weight gain of bare Zry and coated Zry after corrosion in autoclave at 360^{o}C and 18.6MPa for 72h

b) ODS FeCrAl

TEM bright-field images in Figure 7a show two types of grains in ODS FeCrAl. The large grains of above 1 μm in diameter are surrounded by small grains of a few hundred nanometers in diameter. The oxide particles precipitate at grain boundaries and grain interiors. Their distribution is not homogeneous and small particles tend to coarsen. SEM images show that after annealing the elongated grains have evolved into equiaxed subgrains (Figure 7b).

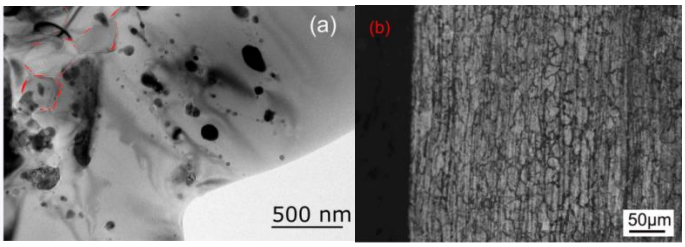

Figure 7: TEM and SEM images of ODS-FeCrAl tube

Mechanical properties of ODS FeCrAl tubes annealed at 600 and 800℃ are given in Figure 8 shows that there are no obvious differences in mechanical properties for tubes and cylinder-type samples.

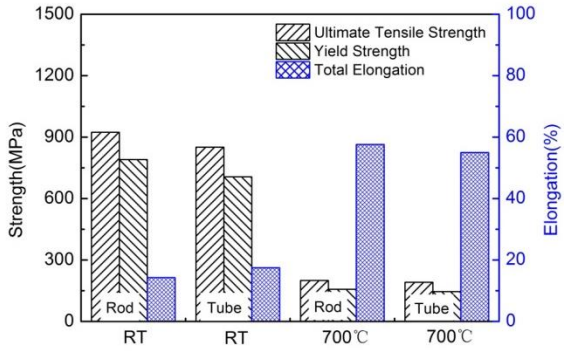

Figure 8: Comparison of mechancial properteis of ODS FeCrAl tube and cylinder-type smaples

Figure 9 shows the weight gain exposure to 1200℃ steam. It can be seen that the ODS FeCrAl had excellent oxidation resistance, which is two orders of magnitude lower than that of Zircaloy, due to the dense oxide film formed on the FeCrAl surface.

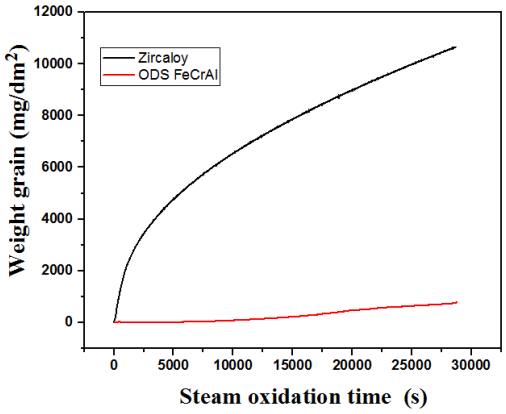

Figure 9: Weight gain of ODS FeCrAl and Zircaloy alloy as a function of time at 1200℃

c) ODS Mo alloy

TEM bright-field images in Figure 10 show that the grains in the ODS Mo tubes have been heavily elongated into a fiber-like structure. The additive has been transformed into nanoscale particles which seem to mostly locate at grain interiors. Dislocation tangles can be observed as well. Appropriate heat treatment could be used to tailor the microstructure to obtain optimum mechanical properties, which is being investigated.

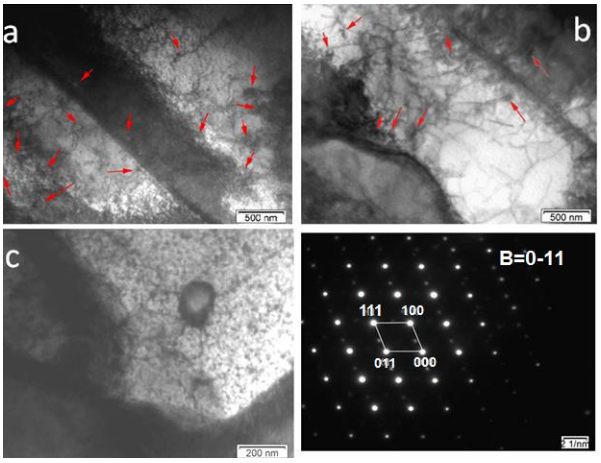

Figure 10: TEM bright-field images of the ODS Mo tubes

The tensile mechanical properties of the ODS Mo alloy tubes have been tested in air at room temperature, 400℃ and 1200℃. The results in Figure 11 show that the ODS Mo maintained sufficient strength at 1200℃, while Zircaloy fully lost its strength at this temperature. This advantage could enable cooling capability of reactor

core, if the ODS Mo alloy is used as fuel cladding.

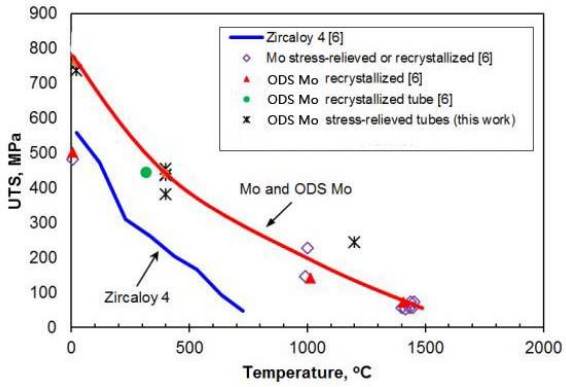

Figure 11: Comparison of mechanical properties of (ODS) Mo and Zircaloy alloy (the literature data are referred to [9])

The compatibility of the FeCrAl coated ODS Mo alloy has been tested either with a PWR water environment to simulate a normal operating condition or with a high temperature steam environment to simulate a LOCA condition. The results show that the coating was not subjected to severe corrosion damages and mass change. On the basis of good out-pile performance, the ODS Mo tubes were put into the research reactor to carry out the test of neutron irradiation. The low-dose irradiated samples had been piled out and were waiting for the examination in hot cell.

d) SiC_f/SiC composite

SiC_f/SiC composites consist of SiC matrix, SiC fibers and PyC interface. The matrix is β-SiC columnar crystals. The PyC interfacial layer is 100-150nm in thickness and the fibers are nano grains. At the interfaces of SiC matrix and fibers, there is PyC layer prepared by chemical vapor infiltration (CVI) process to coordinate the thermal expansion mismatch of matrix and fibers and mitigate thermal stresses induced cracking. In the case of interface-free coating, the free carbon layer on the fiber surfaces has week bonding with the matrix. The PyC layer can resist crack propagation. The HRTEM image in Figure 12 shows that PyC interfaces are anisotropic and parallel to the length direction of the fibers.

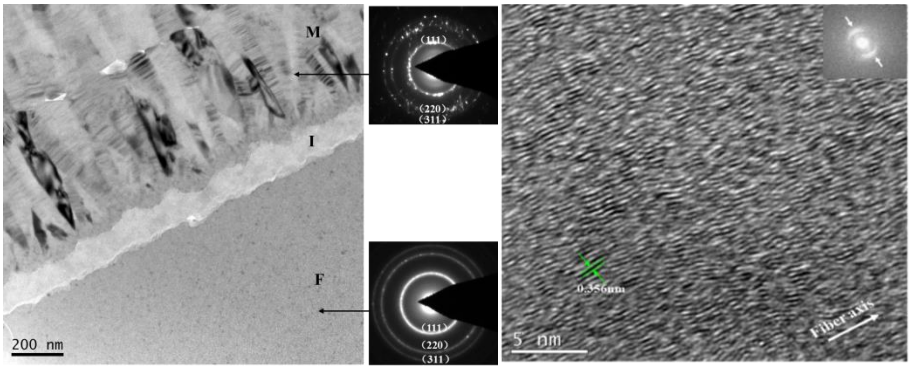

Figure 12: TEM images of the interfaces at matrix/fibers and HRTEM image of PyC interfaces

Figure 13 shows the mechanical properties of SiC_f/SiC composite. Each test repeated 15 times to increase statistic confidence. The ultimate tensile strength and flexural strength are 208MPa at room temperature vs 186MPa at 1200℃, 387MPa at room temperature vs 414MPa at 1200℃, respectively. As shown by these data, SiC_f/SiC composite has good high temperature mechanical properties, similar to the room temperature properties.

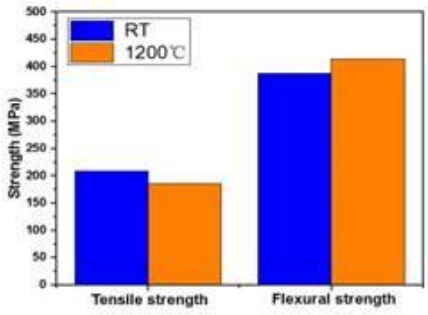

Figure 13: Tensile and flexural strength of SiC_f/SiC composites at room temperature and 1200^oC

The oxidation test under 1200℃ steam for 1h shows that there is no obvious oxidation induced weight gain (Figure 14), instead, slight weight loss can be detected. Compared to Zircaloy, the oxidation rate is three orders of magnitude slower, which the weight gain of Zircaloy and SiC under 1200℃ steam for 1h was 4388mg/dm^2 and -8mg/dm^2 respectively, indicating excellent oxidation resistance of SiC

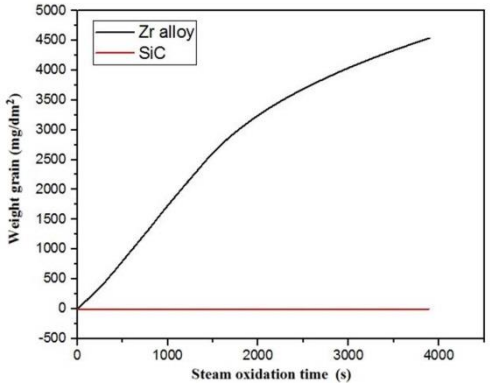

Figure 14: Oxidation weight gain of SiC and Zircaloy exposed to 1200℃ steam as a function of time

e) High thermal conductivity UO_2 pellets

The type and sintering method of high thermal conductivity UO_2 pellets were shown in table 1, with the comparison of SPS and pressureless sintering (PLS). All of the pellets can reach a density about 95% both SPS and PLS.

Table 1: Characteristics of the sintered pellets

Type / Property	UO_2-BeO		UO_2-SiC		UO_2-M	
	SPS	PLS	SPS	PLS	SPS	PLS
Sintering time	0.5 h	24 h	0.5 h	24 h	0.5 h	24 h
Relative density	95±1%	95±1%	95±1%	<95%	95±1%	95±1%

Figure 15 shows the thermal conductivity of the pellets at various temperatures. Compared to traditional UO_2 pellet, the thermal conductivity of the ceramic modified UO_2 has 50% increase at room temperature and 40% increase at 1200℃, the thermal conductivity of the metal modified UO_2 has 70% increase from room temperature to 800℃.

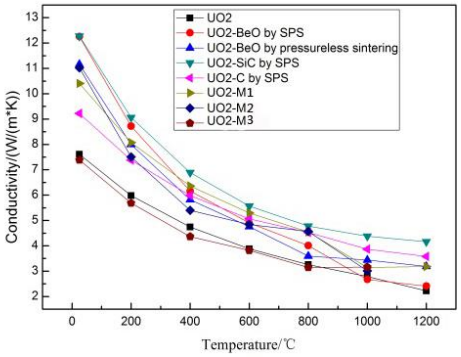

Figure 15: Thermal conductivities of various fuel pellets at different temperature

4. ATF safety and economic performance analyses

a) Typical ATF safety analysis

In order to evaluate the performance of ATF during accident condition, typical large-break LOCA (LBLOCA) design basis accident and station blackout (SBO) accident were chosen to make an assessment. The design basis accident is devoted to determining the safety margins of ATF system, thus, it concerns mainly the peak cladding temperature. The severe accident focuses on the delay cladding failure time.

LBLOCA accident is analyzed using the best-estimate thermal hydraulic system response analysis program RELAP5 and the conservative initial hypothesis method. Figure 16 illustrates the comparison of peak cladding temperature of different fuel systems. It implies that peak cladding temperature of UO_2 (BeO)+FeCrAl is largely lower than that of UO_2-Zr system (910.27℃). This is due to the differences in thermal properties of cladding and fuel, such as thermal conductivity and specific heat. When the cladding oxidation begins, the high oxidation resistance of FeCrAl allows the relevant fuel systems' peak cladding temperature to be much lower than that of the UO_2-Zr system. Under LBLOCA condition, peak cladding temperature of UO_2 (BeO)+FeCrAl fuel system is largely lower than that of UO_2-Zr fuel system. In consideration of the different acceptance criteria, safety margins are increased significantly.

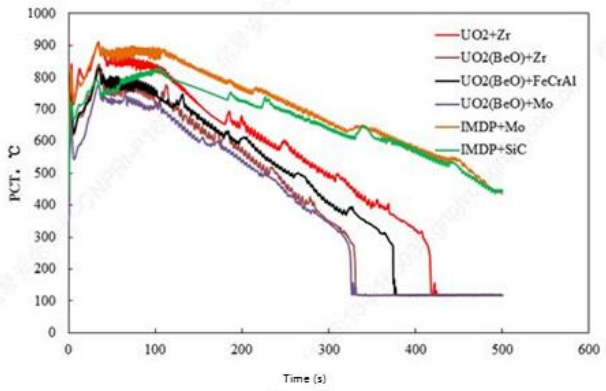

Figure 16: Peak cladding temperature（PCT）under LBLOCA accident

The SBO accident was simulated as a typical severe accident. It assumes that, SBO accident happens at 0s, the RIS system is workable, GCT-a action automatically,

but the pump of ASG disable, and the core outlet temperature reaches 650℃. Three safety valves of regulator are opened manually to release pressure.

In case of an accident, strong oxidation happens on the cladding of UO_2-Zr and UO_2+BeO-Zr fuel systems. The released heat due to cladding oxidation makes cladding temperature increase dramatically until failure. However, the oxidation heat release rate of UO_2+BeO-FeCrA fuel system is slight, thus, cladding temperature increases gently until failure. For this case, cladding temperature does not reach melting point (2730K). It's the long-term oxidation that reduces the cladding thickness and finally leads to fail.

According to the results, four ATF systems IMDP-SiC, IMDP-Mo (FeCrAl coating), UO_2+BeO-FeCrAl and UO_2+BeO-Zr, delay cladding failure for about 113.3min, 66.7min, 41.7min, and 21.7min, respectively. The IMDP-SiC system shows outstanding performance under accident condition. It delays effectively the sequence of events and extends the core melting time, so that more time is gained for the operator to prevent and mitigate the severe accident.

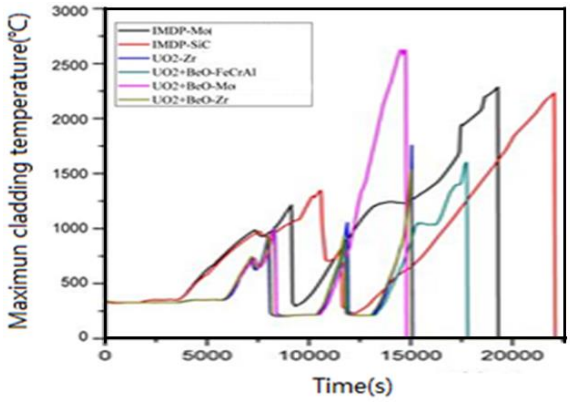

Figure 17: Maximum cladding temperatures

b) ATF typical economic performance

Economic performance of ATF cladding is briefly introduced by taking SiC cladding as an example. SiC is a fully innovative fuel cladding for pressurized water reactors, and the effect of SiC cladding on fuel cycle cost will be focused on the following aspects: (1) the fabrication cost of cladding will be changed, for the reason that the cost of fuel cladding purchase is contained in the cost of fuel assembly fabrication cost. This effect will be reflected by the fuel assembly cost change per unit

uranium; (2) the new type of cladding will influence the dimensions and ^{235}U enrichment of fuel pellets, then the amount of raw material requirement, corresponding conversion cost and amount of separate work unit will be changed; (3) neutron economic performance of fuel assembly by using SiC as its cladding can be improved due to lower thermal neutron absorption cross section[14].

In the following assessment, the design of fuel assembly using SiC as its cladding takes a mature commercial 17x17 PWR fuel assembly as reference (with ^{235}U enrichment assumed to 4.45%, zirconium alloy cladding thickness 0.057cm and pellet radius 0.4096cm) [15]. While fuel height, cladding outer diameter and gap thickness remain the same as the typical PWR fuel assembly, cladding wall thickness, outer diameter of fuel pellet and ^{235}U enrichment should be modified according to thermal, mechanical and neutron physics requirements. According to an advanced fuel designed with SiC cladding by Shannon.M et al.[16], wall thickness of 0.14cm and correspondingly pellet radius of 0.3266cm are adopted in the current SiC-cladding fuel assembly. At present, the cost of SiC cladding is about 8.6 times (3000$/fuel rod) of zirconium alloy, mainly because of its high price of raw material and complicated fabrication process. On the other hand, the cost of zirconium alloy cladding purchase accounts for 15.92% of fuel assembly fabrication, which accounts for 16.05% of the whole fuel cycle cost. Therefore, the fuel cycle cost will be increased by 19.4% because of the increased cladding purchase cost.

Since the pellet radius is reduced by 20% compared to the reference, the ^{235}U enrichment should be increased in order to maintain a similar cycle length. The uranium enrichment for the case of SiC cladding is determined by the criterion of having the same k-infinity value as the reference case at 1100EFPD (Effective Full Power Day) [17], calculated using fuel assembly models with reflective boundaries. Shown in the Figure 18, the current maximum commercial ^{235}U enrichment of 4.95% cannot satisfy the cycle length, as the k-infinity falls far below the reference value, and the ^{235}U enrichment needs further increase to 7.25%. Neutron flux spectra for the reference and SiC-cladding (with 7.25% ^{235}U enrichment) assemblies are plotted in Figure 19 for the thermal and epi-thermal neutron energy regime. It is found that the

fraction of thermal neutron is higher for the SiC-cladding case. In addition, while the thermal neutron spectrum of the reference does not change significantly, the neutron spectrum of the SiC-cladding fuel becomes more thermal during depletion. Care should be taken, as the above higher thermal fraction and consecutive thermalization in the neutron spectrum for the case of SiC-cladding may lead to less negative and even positive moderator temperature coefficient (MTC), as reported by J.J.Power et al.[17].

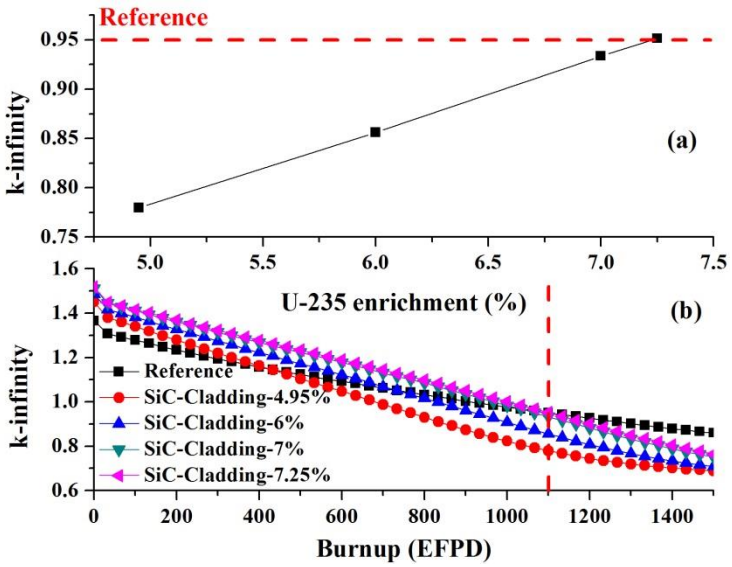

Figure 18: k-infinity changes with U-235 enrichment

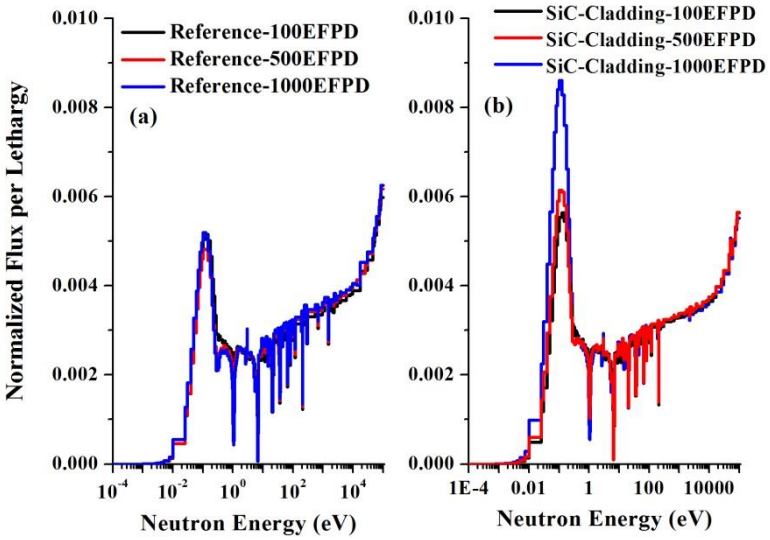

Figure 19: Neutron flux spectrum for the reference and SiC-cladding fuels

Assuming the ^{235}U enrichment to be 7.25% for the SiC-cladding fuel, the amount

of raw material and separate work unit will be increased by % and % respectively . Taking all the factors mentioned above into consideration, together with the percentage of raw material, conversion and enrichment, the whole fuel cycle cost will be increased by%. Combined with the 19.4% increase in the cost of cladding the fuel cycle cost of assembly with SiC cladding will be increased by 8.3%, compared to the reference commercial fuel assembly,.

Though the current SiC-cladding fuel needs ^{235}U enrichment of 7.25%, due to the smaller heavy metal inventory, neutron economic performance of fuel assembly can be improved by using SiC as its cladding. As shown in Figure 20, thermal neutron absorption cross section is about 50% lower for SiC. N.M.Geogre et al. has compared neutron economic performance of fuels with different claddings, and found that the required ^{235}U enrichment can be reduced when Zircaloy is replaced by SiC. Further improvement on economics can be expected, when thinner SiC cladding with high performance satisfying thermal and mechanical requirement is developed in the future.

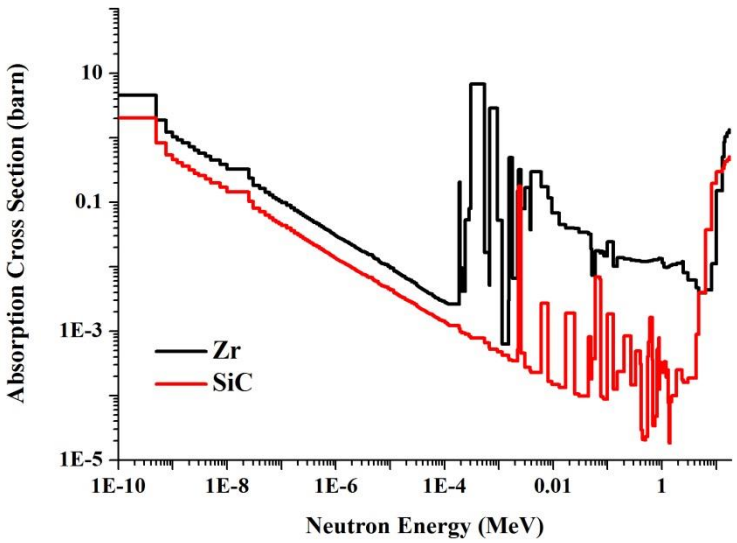

Figure 20: Neutron absorption cross section of Zr and SiC

5. Conclusions

ATF candidate claddings and pellets including surfaced-coated zirconium alloy, iron-chromium-aluminum alloys, coated molybdenum alloy, silicon carbide claddings

and high thermal conductivity UO_2 pellets, have been developing by CGN[11-13]. The out-of pile performances of these candidates such as thermal and mechanical properties and high temperature corrosion have been tested. In parallel the economic evaluation and safety analysis have been carried out for typical ATF designs.

Acknowledgments

The authors are grateful to the financial support from China National Science and Technology Major Special Project "Research on Accident Tolerant Fuels Key Technologies" (Grant No. R-2015ZBNFC003), China CGN Strategic Special Project for Scientific and Technological Innovation "Fundamental Research on Accident Tolerant Fuels" (R-2015ZBNFC001), the National Natural Science Foundation of China (51502322) and the National Key Research and Development Program of China (2017YFB0702404).

References

[1] S.J. Zinkle, K.A. Terrani, J.C. Gehin, L.J. Ott, L.L. Snead, J. Nucl. Mater. 448 (2014) 374-379.

[2] S. Briggs-Sitton, Nucl. News (March) (2014) 83-91.

[3]X. Gong, R. Li, M.Z. Sun, Q.S. Ren, T. Liu, M.P. Short, J. Nucl. Mater. 482 (2016) 218-228.

[4] Hyun-Gil Kim, Il-Hyun Kim, Yang-Il Jung, Dong-Jun Park, Jeong-Yong Park, Yang-Hyun Koo, J. Nucl. Mater. 465(2015)531-539.

[5] Short, M.P, Multilayer Composite Fuel Cladding for LWR Performance Enhancement and Severe Accident Tolerance. https://neup.inl.gov/SiteAssets/FY%202015%20Abstracts/R_D/NEUP_Attachments Proposal_CFA-15-8347_Filtered.pdf, 2016.

[6] Y. Yamamoto, B.A. Pint, K.A. Terrani, K.G. Field, Y. Yang, L.L. Snead, J. Nucl. Mater. 467(2015)703-716.

[7] B. Cheng, P. Chou, Y-J. Kim, Nucl. Sci. Tech. 2016. 2(5): 1-6.

[8] B. Cheng, Y-J. Kim, P. Chou, Nucl. Eng. Tech. 48 (2016) 16-25.

[9] B. Cheng, Program on Technology Innovation: Coated Molybdenum-Alloy Cladding for Accident-Tolerant Fuel Progress Report. 2015, EPRI.

[10] C.P. Deck, G.M. Jacobsen, J. Sheeder, O. Gutierrez, J. Zhang, J. Stone, H.E. Khalifa, C.A. Back, J. Nucl. Mater. 466 (2015)667-681.

[11] Weichao Bao, Jiaxiang Xue, Ji-Xuan Liu, Xingang Wang, Yifeng Gu, Fangfang Xu, Guo-Jun Zhang, Journal of Alloys and Compounds 730 (2018) 81-87.

[12] Xing Gong, Sigong Li, Rui Li, Jun Yan, Jiaxiang Xue, Qisen Ren, Tong Liu, 2017 Top Fuel.

[13] Bai Guanghai, Chen Zhilin, Zhang Yanwei, Liu Erwei, Xue Jiaxiang, Yu Weiwei, Wang Rongshan, Li Rui, Liu Tong，RARE METAL MATERIALS AND ENGINEERING，2017（7），2035-2040.

[14] Nathan.Michael.George, Kurt.Terrani, Jeff.Powers et al., Neutronic analysis of candidate accident-tolerant cladding concepts in pressurized water reactors, Annals of Nuclear Energy, 75(2015)703.

[15] Xu.Wu, Tomasz.Kozlowski, Jason.D.Hales, Neutronics and fuel performance evaluation of accident tolerant FeCrAl cladding under normal operation, Annals of Nuclear Energy, 85(2015)763.

[16] Shannon M.Bragg-Sitton. Advanced LWR nuclear fuel cladding system development technical program plan. Light water reactor sustainability program, 2012

[17] J.J.Powers, W.J.Lee, F.Venneri et al., Fully ceramic microencapsulated (FCM) replacement fuel for LWRs, ORNL/TM-2013/173.